JACS
JOURNAL OF THE AMERICAN CHEMICAL SOCIETY
Article
pubs.acs.org/JACS

Pyridalthiadiazole-Based Narrow Band Gap Chromophores

Zachary B. Henson,[#,†,§] Gregory C. Welch,[#,†,‡,§] Thomas van der Poll,[‡,§] and Guillermo C. Bazan*[,†,‡,§]

[†]Center for Polymers and Organic Solids, [‡]Center for Energy Efficient Materials, and [§]Department of Chemistry & Biochemistry, University of California, Santa Barbara, California 93106, United States

Supporting Information

ABSTRACT: π-Conjugated materials containing pyridal-[2,1,3]thiadiazole (PT) units have recently achieved record power conversion efficiencies of 6.7% in solution-processed, molecular bulk-heterojunction (BHJ) organic photovoltaics. Recognizing the importance of this new class of molecular systems and with the aim of establishing a more concrete path forward to predict improvements in desirable solid-state properties, we set out to systematically alter the molecular framework and evaluate structure−property relationships. Thus, the synthesis and properties of 13 structurally related D^1-PT-D^2-PT-D^1 compounds, where D represents a relatively electron-rich aromatic segment compared to PT, are provided. Physical properties were examined using a combination of absorption spectroscopy, cyclic voltammetry, thermal gravimetric analysis, differential scanning calorimetry, and solubility analysis. Changes to end-capping D^1 units allowed for fine control over electronic energy levels both in solution and in the bulk. Substitution of different alkyl chains on D^2 gives rise to controllable melting and crystallization temperatures and tailored solubility. Alterations to the core donor D^2 lead to readily identifiable changes in all properties studied. Finally, the regiochemistry of the pyridal N-atom in the PT heterocycle was investigated. The tailoring of structures via subtle structural modifications in the presented molecular series highlights the simplicity of accessing this chromophore architecture. Examination of the resulting materials properties relevant for device fabrication sets forth which can be readily predicted by consideration of molecular structure and which lack a systematic understanding. Guidelines can be proposed for the design of new molecular frameworks with the possibility of outperforming the current state of the art OPV performance.

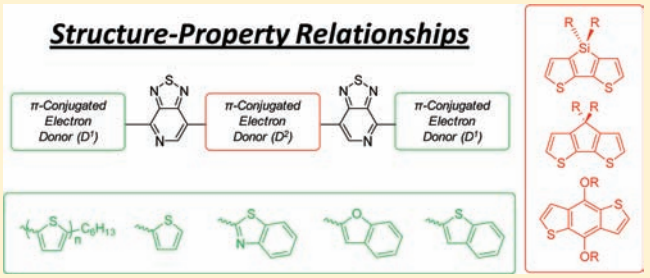

INTRODUCTION

Organic π-conjugated materials have found wide application as active components in a variety of optoelectronic devices,[1] including light emitting diodes,[2−4] field effect transistors,[5−7] solar cells,[8−10] optical sensors,[11] electrochromic devices,[12−14] and photodetectors.[15] Properties important to achieve these functions include the ability to act as semiconductors and to absorb and emit light within specific regions of the spectrum. In addition, organic semiconductors offer the ability to be processed by thermal evaporation[16−19] at moderate temperatures or via solution deposition methods,[9,20,21] thus allowing for mild processing procedures and the integration of lightweight, flexible substrates into the device architecture.[22−24] Furthermore, the optical, electronic, and solid-state organizational tendencies of organic π-conjugated systems can be systematically modified through molecular design.[25−28]

Organic photovoltaic (OPV) devices prepared via solution methods are of substantial current interest. Much of the recent and current literature concerns the use of conjugated polymer donors in combination with fullerene acceptors and how these materials can form "bulk heterojunction" (BHJ) phase-separated active thin films within the solar cell architecture.[29−34] One advantage of using polymers is their desirable film-forming properties.[9] Additionally, π-conjugated polymers exhibit extended electronic delocalization along their backbones, leading to long wavelength light absorption and good charge carrier mobilities.[35−40]

Less work has appeared on OPV materials with small or intermediate sized molecules, for which the formation of smooth and stable films is more challenging than with their polymeric analogues. However, π-conjugated molecular systems offer several possible advantages compared to π-conjugated polymers, in that they can be readily purified using standard organic chemistry methods, and their structural features can be more precisely verified.[41−44] Additionally, due to their monodisperse nature, molecular alternatives minimize the batch-to-batch variability sometimes encountered with polymers and provide model compounds for detailing more precise structure−property relationships.[45,46]

Examples of solution-deposited molecular OPV materials have been reported that include the following structural units: merocyanine,[47,48] squaraine,[18,49−52] and BODIPY dyes,[53−55] isoindigo,[56] and diketopyrrolopyrrole[57,58] based chromophores, linear[59−61] and star-shaped oligothiophenes,[62−64] and push−pull organic dyes.[65] Recently, we reported the synthesis and characterization of a new molecular architecture built upon pyridal[2,1,3]thiadiazole (PT) and dithieno(3,2-*b*;2′,3′-*d*)silole

Received: October 4, 2011
Published: January 27, 2012

   dx.doi.org/10.1021/ja209331y | *J. Am. Chem. Soc.* 2012, 134, 3766−3779

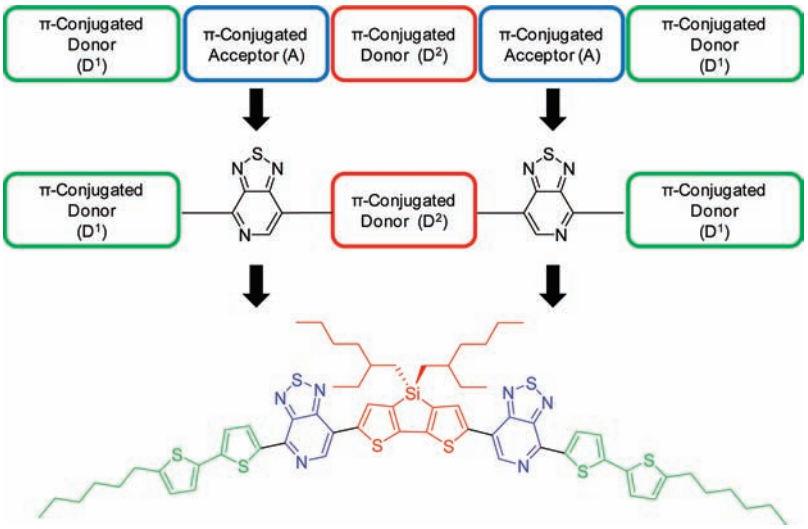

Figure 1. Cartoon depiction of the general D^1-A-D^2-A-D^1 chromophore framework, the role of PT as the acceptor (A) component of the conjugated framework, and a specific molecular example.

Scheme 1. General Synthetic Entry into D^1-PT-D^2-PT-D^1 Molecules 1−7 with Modified End-Capping D^1 Units[a]

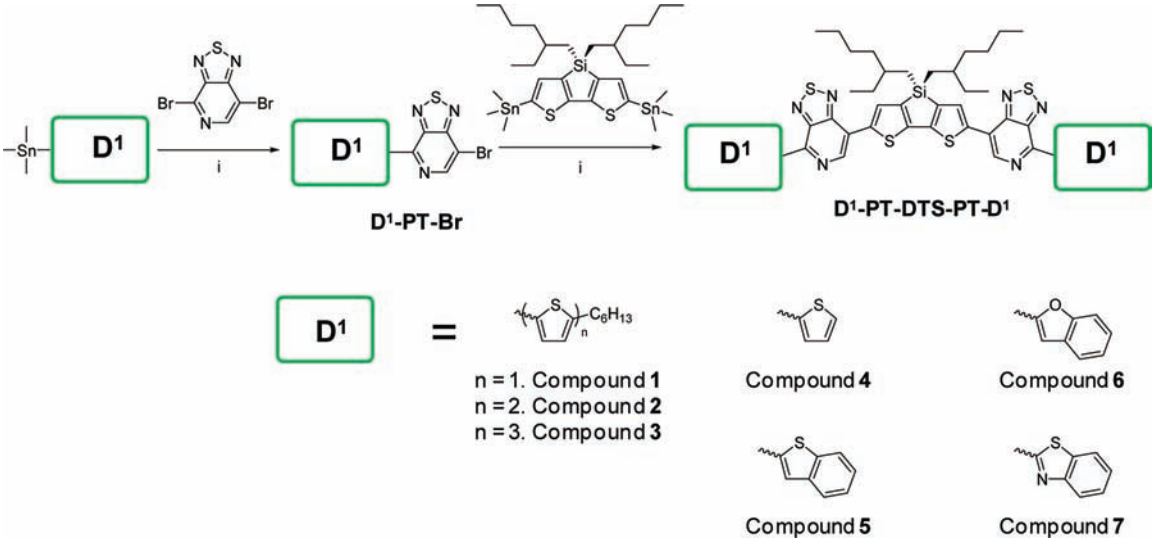

[a]Conditions: (i) microwave heating, 175 °C, 60 min, cat. $Pd(PPh_3)_4$, toluene.

(DTS) structural units.[66] These molecules are of intermediate dimensions and have found utility as the donor phase in solution processed small molecule BHJ solar cells with power conversion efficiencies (PCEs) reaching upward of 6.7%, the highest reported to date.[67] One example, 5,5′-bis{7-(4-(5-(hexylthiophen-2-yl)thiophen-2-yl))[1,2,5]thiadiazolo[3,4-*c*]-pyridine}-3,3′-di-2-ethylhexylsilylene-2,2′-bithiophene, shown in Figure 1, corresponds to a class of conjugated molecules that can be generally described by a D^1-A-D^2-A-D^1 conjugated framework. D and A correspond to electron rich and poor aromatic moieties, respectively, which lead to charge transfer excited states and absorption characteristics useful for OPV integration. Within this architecture, pyridal[2,1,3]thiadiazole (PT) corresponds to "A". Incorporating PT within the structural design is also practical from the perspective of elaborating different chromophore structures via streamlined synthetic approaches.[66]

In this contribution, we examine a range of D^1-PT-D^2-PT-D^1 structures with the goal of establishing how structural variations influence orbital energy levels, solubility characteristics, and thermal transitions. Our goal is to provide an understanding of the molecular basis for these properties. We recognize that other considerations, including morphology, miscibility of multiple components, deposition strategies, etc., are necessary for successful device fabrication.[68−70] This manuscript is, however, chemistry-centric and is organized in the following way. First, we show how variations of D^1 allow control over the optical and electronic properties of the molecule. Next, we examine the role of solubilizing alkyl chains on the central D^2 unit as a means of controlling solubility and thermal behavior in the bulk. Additionally, we incorporate two other well-known donor units as the central D^2 building block and examine relevant properties. Finally, we explore the influence of the pyridal N-atom regiochemistry.[71] As will become apparent, each component influences the final molecule's electronic, optical, and physical properties to various degrees, providing multiple design opportunities. We anticipate that the structure−property relationships revealed in this study have

dx.doi.org/10.1021/ja209331y | *J. Am. Chem. Soc.* 2012, 134, 3766−3779

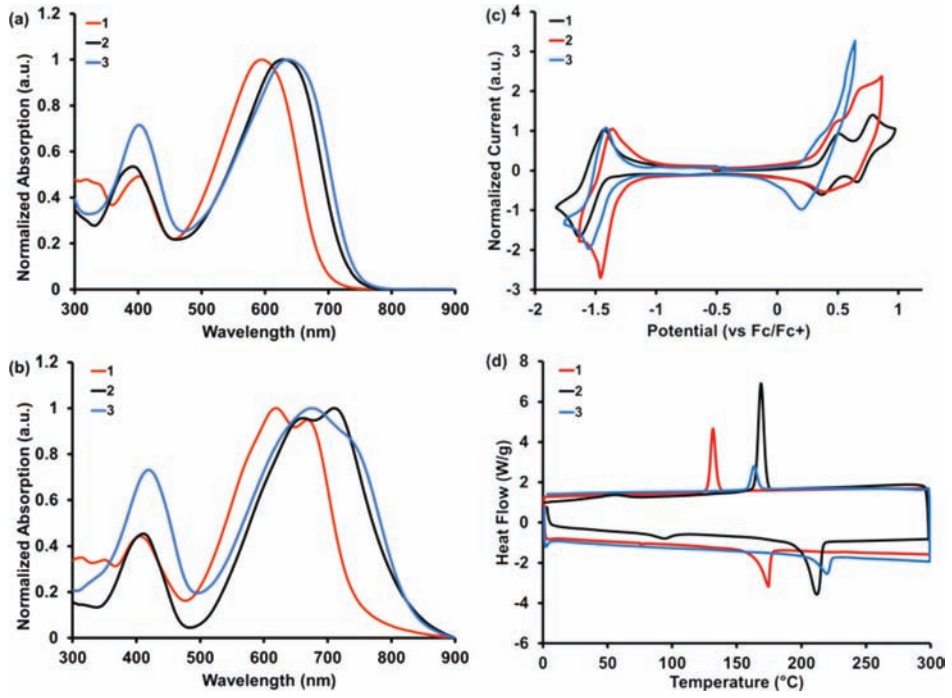

Figure 2. (a) Normalized optical absorption spectra of **1**, **2**, and **3** in (a) $CHCl_3$ solution and (b) thin films on quartz. (c) Cyclic voltammetry plots obtained in CH_2Cl_2 solution. (d) Differential scanning calorimetry plots of molecules containing different terminal D^1 units.

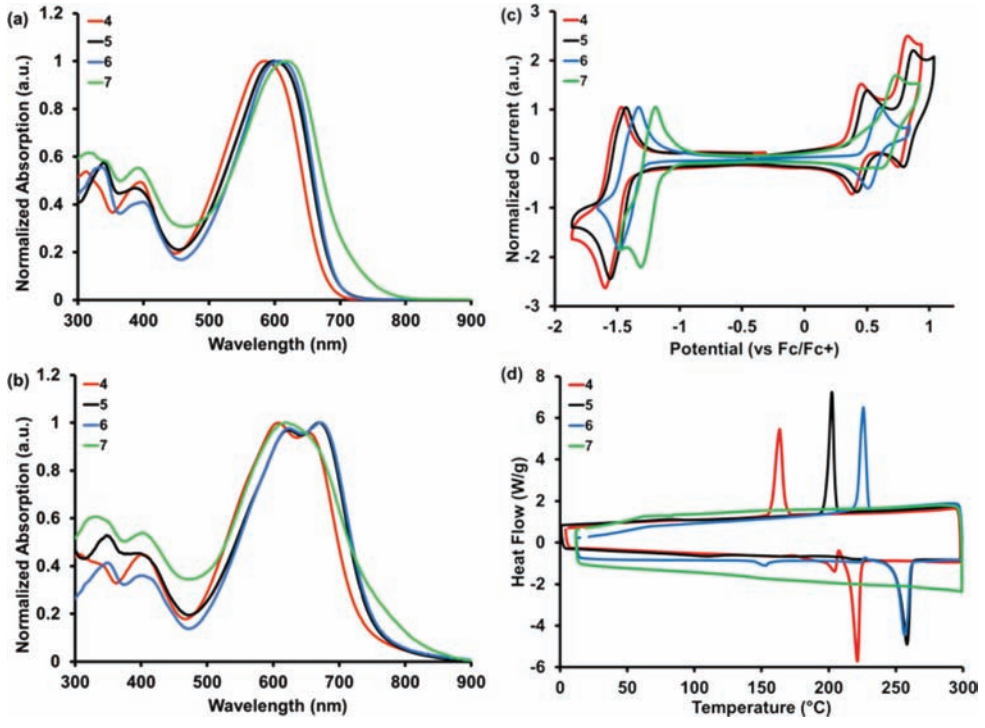

Figure 3. (a) Normalized optical absorption spectra of **4**, **5**, **6**, and **7** in (a) $CHCl_3$ solution and (b) thin films on quartz. (c) Cyclic voltammetry plots obtained in CH_2Cl_2 solution. (d) Differential scanning calorimetry plots of molecules containing different terminal D^1 units.

the potential to translate to other molecular architectures and to maximize efficiency in the pursuit of more promising candidates. It is also worth noting that the structural precision in the oligomers examined here allows us to better correlate variations in molecular connectivity with relevant properties, when compared with -$[D\text{-}A]_n$- conjugated polymers, for which aggregation, polydispersity, and molecular weight variations can obfuscate the role of molecular design.[37,72−74]

RESULTS AND DISCUSSION

1.1. Variation of Terminal Donor Groups (D^1).

Molecular Structures and Synthetic Approach. Scheme 1 shows a series of compounds containing a PT-DTS-PT core and various aromatic end units, i.e. compounds **1**−**7**. These include alkylated fragments, such as hexylthiophene (**1**), hexylbithiophene (**2**, which corresponds to the example in

Table 1. Summary of λ_{max}, λ_{onset}, and E_{gap} for Compounds 1−13 in Solution and as Thin Films

		UV−vis solution[a]			UV−vis thin film[b]		
	compd	λ_{max} (nm)	λ_{onset} (nm)	E_{gap} (eV)	λ_{max} (nm)	λ_{onset} (nm)	E_{gap} (eV)
alkyl thiophene (D^1)	1	600	690	1.80	620	760	1.63
	2	625	732	1.69	720	820	1.51
	3	645	740	1.67	680	820	1.51
planar (D^1)	4	582	678	1.83	604	754	1.64
	5	595	695	1.78	664	760	1.63
	6	605	696	1.78	670	765	1.62
	7	620	750	1.65	625	780	1.59
alkyl chain	8	625	732	1.69	720	785	1.58
	9	625	732	1.69	720	800	1.55
donor core (D^2)	10	555	650	1.90	585	715	1.73
	11	620	716	1.73	628	760	1.63
regioisomers	12	655	715	1.73	725	815	1.52
	13	625	715	1.73	645	810	1.53

[a] $CHCl_3$ was used as the solvent. [b] As-cast from $CHCl_3$ on quartz.

Figure 1), and hexyltrithiophene (**3**), along with the unsubstituted planar aromatic units thiophene (**4**), benzothiophene (**5**), benzofuran (**6**), and benzothiazole (**7**). This series of compounds was chosen to probe the influence of extended π-conjugation (**1**−**3**) and increased electron affinity (**4**−**7**) across the molecular backbone.[45,58]

Some brief comments on the synthesis follows. Complete information can be found in the Supporting Information. All the building blocks are commercially available or can be easily prepared. The general synthetic strategy is shown in Scheme 1. The initial step involves a Stille cross coupling reaction between a stannylated terminal fragment and 4,7-dibromo-pyridal-[2,1,3]thiadiazole to provide D^1-PT-Br in yields in excess of 70%. Excellent regioselectivity at the C−Br postion adjacent to the pyridal N-atom of 4,7-dibromopyridal[2,1,3]thiadiazole is obtained.[75,76] Subsequent reaction of D^1-PT-Br with the distannylated DTS reagent yields the desired compounds. Microwave heating typically provided higher yields than conventional heating methods and reduced reaction times.[72] The products were purified using silica gel column chromatography and/or precipitation into a poor solvent to afford purple or red solids that are soluble in common organic solvents. Purity was determined by solution NMR spectroscopy, mass spectrometry, and elemental analysis.

1.2. Optical Characterization. As shown in Figures 2a and 3a, and as summarized in Table 1, $CHCl_3$ solutions of **1**−**7** exhibit broad optical absorption with distinct high and low energy bands attributed to localized π−π^* and internal charge-transfer transitions, respectively. Such absorption profiles are typical of donor−acceptor type π-conjugated molecules.[25,77] An approximately 40 nm red shift in the onset of absorption (λ_{onset}) is observed when comparing **1** and **2**, consistent with the increased conjugation length afforded by the two additional thiophene moieties.[45] Increasing the number of thiophene units in D^1 to 3 (**3**) results in only a slight red shift of λ_{onset} (8 nm) when compared to **2**. This observation indicates that the narrowing of the optical band gap afforded by the number of thiophene units in the D^1 fragment saturates between two and three repeat units.

Normalized thin film absorption spectra of compounds **1**, **2**, and **3** are shown in Figure 2b. These films were prepared by spin coating 1% (w/v) $CHCl_3$ solutions onto quartz substrates. Comparison of parts a and b of Figure 2 shows that transitioning from solution to solid state gives rise to a red shift in λ_{onset} of 70, 88, and 80 nm for compounds **1**, **2**, and **3**, respectively, together with the emergence of more than one band in the low energy transition region. We attribute these observations to through space interactions (such as electron exchange and dipole−dipole) in the solid state.[78,79] It is interesting to point out that the relative strength of the two peaks for **2** is biased toward the lower energy component, whereas the opposite is true for **1** and **3**. The stronger absorbance at larger λ for **2** relative to **3** suggests a higher fraction of chromophores in a well-ordered phase in as-cast films. This is supported by an enlargement of the low energy peak upon thermal annealing of all films (Supporting Information). Optical band gaps were determined from λ_{onset} to be 1.63, 1.51, and 1.51 eV for **1**, **2**, and **3**, respectively.

Normalized absorption spectra of **4**−**7** are shown in Figure 3a and 3b. As shown by **4**, removing the hexyl substituents from the terminal thiophene in **1** results in a slight blue shift (<20 nm) in the absorption maximum (λ_{max}) and λ_{onset} in both $CHCl_3$ solution and as a film; see Table 1. Although a weaker donor, introducing benzothiophene as D^1 (**5**) increases the π-conjugation length along the molecular backbone, relative to thiophene, and as a result, a red shift in the solution optical absorption spectrum of **5** is observed when compared to the case of **4**. Oxygen for sulfur substitution in the terminal heterocycle (**5** vs **6**) has minimal impact on the optical properties in solution. Compound **7**, which incorporates benzothiazole for D^1, has the furthest red-shifted spectrum in $CHCl_3$, with a λ_{max} of 600 nm and λ_{onset} at 750 nm. The thin film absorption spectra of **4**−**7** exhibit large red shifts when compared to their corresponding solution spectra. Surprisingly, while **4**, **5**, and **6** display distinct additional features in the low energy absorption bands, as previously attributed to molecular aggregation, only a minimal red shift with no additional features is observed for compound **7**, suggesting that as-cast films do not contain a large fraction of highly ordered domains. As with **1**−**3**, thermal annealing leads to a growth of the longer λ component for compounds **4**−**7** (Supporting Information). The trends in increasing λ_{onset} from **4** to **7** are the same for both the solution and thin film absorption spectra. The optical band gaps were estimated at 1.64 (**4**), 1.63 (**5**), 1.62 (**6**), and 1.59 eV (**7**). From this composite set of data, it is apparent that the band gap within the D^1-PT-D^2-PT-D^1 series can be progressively red-shifted by increasing the conjugation length and/or decreasing the donor ability of D^1. With respect to the

dx.doi.org/10.1021/ja209331y | J. Am. Chem. Soc. 2012, 134, 3766−3779

Table 2. HOMO, LUMO Energy Levels and E_{gap} Determined by Cyclic Voltammetry and Theoretical Calculations for Compounds 1−13

		cyclic voltammetry[a]			DFT calculations[b]		
	compd	HOMO (eV)	LUMO (eV)	E_{gap} (eV)	HOMO (eV)	LUMO (eV)	E_{gap} (eV)
alkyl thiophene (D^1)	**1**	−5.20	−3.48	1.73	−4.87	−2.97	1.90
	2	−5.16	−3.61	1.55	−4.76	−2.99	1.77
	3	−5.07	−3.55	1.52	−4.73	−3.02	1.71
planar (D^1)	**4**	−5.20	−3.47	1.73	−4.98	−3.05	1.93
	5	−5.26	−3.55	1.71	−5.06	−3.13	1.93
	6	−5.34	−3.60	1.74	−5.01	−3.10	1.90
	7	−5.42	−3.75	1.67	−5.28	−3.27	2.01
alkyl chain	**8**	−5.15	−3.59	1.56	−4.76	−2.99	1.77
	9	−5.19	−3.57	1.62	−4.76	−2.99	1.77
donor core (D^2)	**10**	−5.23	−3.51	1.72	−5.09	−2.99	2.10
	11	−5.17	−3.57	1.59	−4.82	−2.97	1.77
regioisomers	**12**	−5.20	−3.60	1.60	−4.82	−3.07	1.74
	13	−5.19	−3.57	1.62	−4.79	−3.02	1.77

[a]HOMO = $-e(4.88\ \text{V} + E_{ox}^{Fc/Fc+})$, where $E_{ox}^{Fc/Fc+}$ = oxidation onset vs ferrocene. LUMO = $-e(4.88\ \text{V} + E_{red}^{Fc/Fc+})$, where $E_{red}^{Fc/Fc+}$ = reduction onset vs ferrocene. [b]From geometry optimized structures determined at the B3LYP/6-31G(d,p) level of theory.

Table 3. Melting Transition Temperature (T_m), Crystallization Transition Temperature (T_c), and Solubility in $CHCl_3$ for Compounds 1−13

		differential scanning calorimetry[a]		thermogravimetric analysis[b]	
	compd	T_m (°C)	T_c (°C)	T_d (°C)	solubility in $CHCl_3$ (mg/mL)
alkyl thiophene (D^1)	**1**	173	132	396	>50
	2	210	169	411	31−35
	3	219	164	410	7−10
planar (D^1)	**4**	221	164	419	27−31
	5	258	203	427	<5
	6	260	208	405	<10
	7	N/A	N/A	299	<10
alkyl chain	**8**	215	185	428	<10
	9	160	124	413	37−43
donor core (D^2)	**10**	270	250	351	18−22
	11	N/A	N/A	396	>50
regioisomers	**12**	207	168	415	>25
	13	202	157	408	>25

[a]Scanned samples at a rate of 10 °C/min from 0 to 300 °C. [b]Samples were run under N_2 and heated from 20 to 800 °C at a rate of 20 °C/min.

latter, a simplistic view involves a primary A′-D^2-A′ chromophore, wherein the acceptor ability of A′ is diminished when PT is adjacent to a D^1 with stronger donor qualities.

1.3. Electrochemical Characterization. Cyclic voltammetry (CV) in CH_2Cl_2 with tetrabutylammonium hexafluorophosphate as the supporting electrolyte was used to evaluate the electrochemical characteristics of **1**−**7**. Figures 2c and 3c show the resulting CV traces. From these data one observes that each D^1-PT-D^2-PT-D^1 molecule exhibits a fully reversible reduction wave, which is reasonably attributed to the presence of the PT fragments,[80] and reversible or quasi-reversible oxidation waves. The highest occupied molecular orbital (HOMO) and lowest unoccupied molecular orbital (LUMO) energy levels were estimated from the onset of the oxidation and reduction waves, respectively (see Supporting Information and Table 2). A higher degree of accuracy is available with these compounds, relative to similar energy level estimates on conjugated polymer films, as the measurements can be carried out in solution.[81] This analysis shows that **1**−**7** have relatively low-lying LUMO energy levels (−3.47 to −3.75 eV). Comparing compounds **1** to **3**, the energy of the HOMO level increases with increasing thiophene chain length from −5.20 eV for **1** to −5.07 eV for **3**. Oxidation is therefore more facile and more readily accommodated by the increased π-conjugation length and electron density across the backbone afforded by the additional thiophene units. Interestingly, changes in the LUMO energy levels do not scale with the number of thiophene fragments, thus reflecting two competing consequences of extending thiophene chain length. Specifically, by comparing **1** and **2**, one finds that increasing the thiophene repeat units from **1** to **2** lowers the energy of the LUMO by ∼0.14 eV, a result of greater electronic delocalization afforded by the extended π-conjugation. Adding another thiophene to the D^1 unit (**2** vs **3**) does not give rise to further lowering; indeed, the energy of the LUMO actually increases by ∼0.06 eV, most likely as a result of the increase in electron density on the conjugated backbone afforded by the two additional thiophene units. The electrochemical band gaps (1.73 eV (**1**), 1.55 eV (**2**), and 1.52 eV (**3**)) are in agreement with the trends observed from absorption measurements: band gap reduction is significant (0.18 eV) when comparing **1** and **2**, while the band gap reduction is less significant (0.03 eV) for **2** vs **3**.

Compounds **4** and **5** have similar HOMO energy levels, see Table 2, with the HOMO of **5** being slightly deeper (−5.20 vs

dx.doi.org/10.1021/ja209331y | J. Am. Chem. Soc. 2012, 134, 3766−3779

Scheme 2. General Synthetic Entry into D^1-PT-D^2-PT-D^1 Molecules 2, 8, and 9 with Modified Alkyl Substituents on a DTS D^2 Fragment[a]

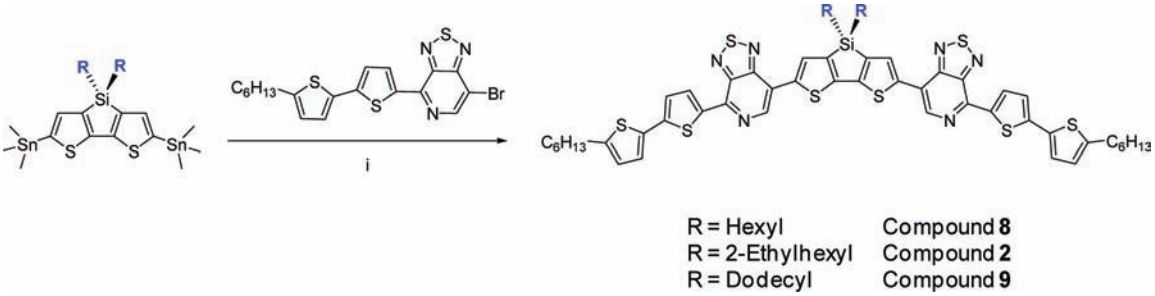

[a]Conditions: (i) Microwave heating, 175 °C, 60 min, cat. $Pd(PPh_3)_4$, toluene.

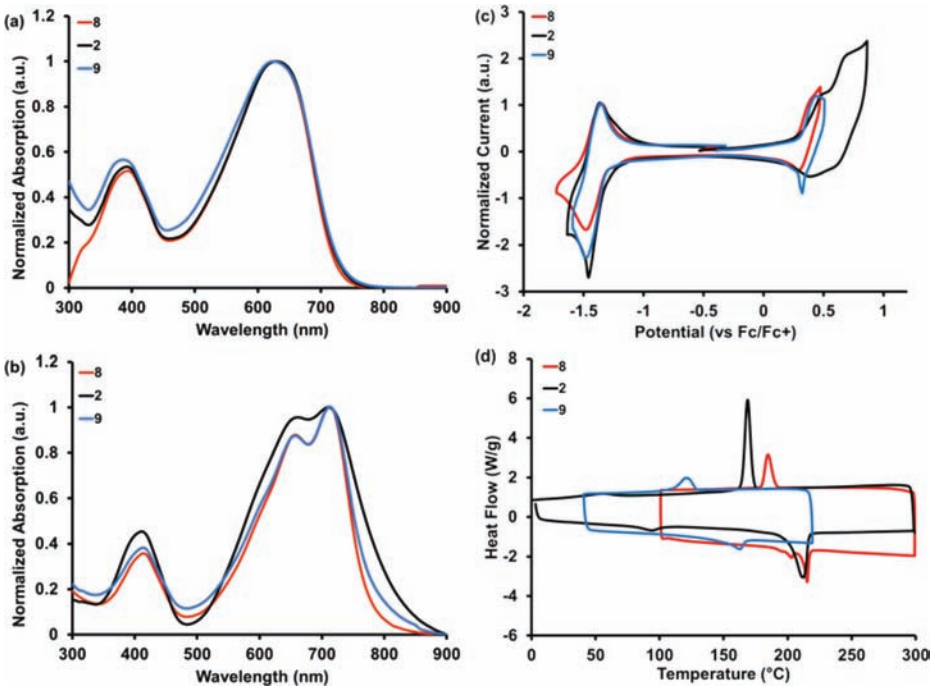

Figure 4. (a) Normalized optical absorption spectra of **2**, **8**, and **9** in (a) $CHCl_3$ solution and (b) thin films on quartz. (c) Cyclic voltammetry plots obtained in CH_2Cl_2 solution. (d) Differential scanning calorimetry plots of molecules with varying D^2 solubilizing alkyl chains.

−5.26 eV). Increasing the electron affinity of D^1 in going from benzothiophene to benzofuran to benzothiazole results in a systematic lowering of the HOMO energy level, with compound **7** having the deepest HOMO (−5.42 eV). The same trend is observed for the LUMO energy levels. Increasing the size of the π-conjugated framework lowers the LUMO energy by ∼0.08 eV when comparing compounds **4** (−3.47 eV) and **5** (−3.55 eV), while replacing the benzothiophene S-atom of **5** with a more electronegative O-atom further lowers the LUMO energy by ∼0.05 eV to −3.60 eV for **6**. Compound **7** with two benzothiazole D^1 units exhibits a significantly lower LUMO energy (−3.75 eV). The electrochemical band gaps were found to be 1.73 eV (**4**), 1.71 eV (**5**), 1.74 eV (**6**), and 1.67 eV (**7**). Overall, these CV measurements indicate to what degree the energy levels of the frontier molecular orbitals can be tailored by altering the conjugation length and/or electron affinity of the D^1 units.

1.4. Thermal Characterization and Solubility Characteristics. Differential scanning calorimetry (DSC) and thermal gravimetric analysis (TGA) were used to probe thermal properties and stabilities, respectively. DSC traces of **1**, **2**, and **3** are shown in Figure 2d, while TGA plots can be found in the Supporting Information. All relevant data are summarized in Table 3. Melting transitions were observed at 173, 210, and 219 °C for **1**, **2**, and **3**, respectively. Thus, as the size of the molecule increases, a higher temperature is required to disrupt crystallinity. Compounds **1**, **2**, and **3** crystallize at 132, 169, and 164 °C, respectively. The higher crystallization temperatures of **2** and **3** compared to **1** may be attributed to the longer π-conjugated structure, which likely favors tighter intermolecular $\pi-\pi$ stacking. All compounds exhibit good thermal stabilities in N_2, showing 5% decomposition at 396 °C (**1**), 411 °C (**2**), and 410 °C (**3**).

DSC traces of **4**−**7** are shown in Figure 3d. Compounds **5** and **6**, with the fused aromatic D^1 units, exhibit significantly higher melting and crystallization temperatures when compared to **4**, which has terminal thiophene units. No obvious thermal transitions were observed for **7** from 0 to 300 °C. The higher temperature transitions of **4**−**6** compared to **1**−**3** are consistent with a reduction in molecular conformational disorder afforded by the more rigid and planar π-conjugated structure and the absence of alkyl substituents on D^1. Compounds **4**, **5**, and **6** are

dx.doi.org/10.1021/ja209331y | J. Am. Chem. Soc. 2012, 134, 3766−3779

Scheme 3. General Synthetic Entry into D^1-PT-D^2-PT-D^1 Molecules 1, 10, and 11 with Modified D^2 Cores[a]

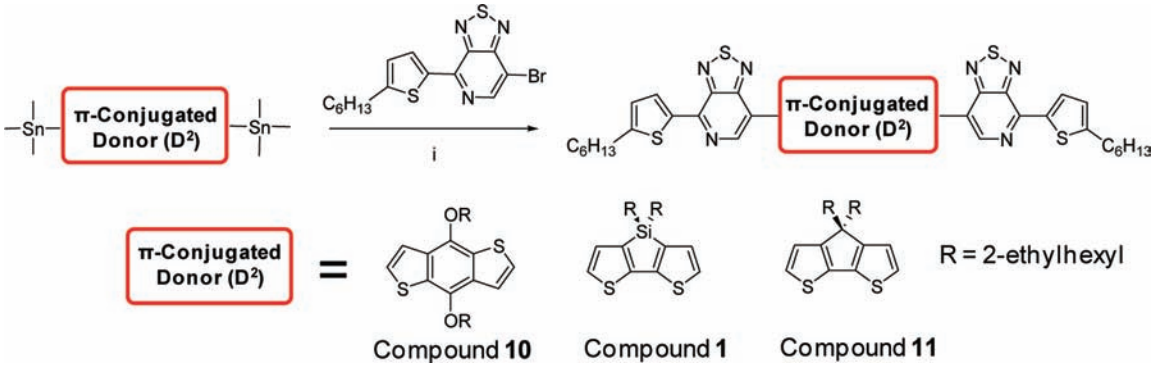

[a]Conditions: (i) Microwave heating, 175 °C, 60 min, cat. $Pd(PPh_3)_4$, toluene.

all thermally stable above 400 °C under a N_2 atmosphere. However, compound **7** shows 5% mass loss at ~300 °C. Therefore, within the current chromophore design guidelines, the benzothiazole unit appears to impart thermal instability when introduced as D^1.

The solubility at room temperature of **1**–**3** in $CHCl_3$ was determined via standard procedures (see Supporting Information) and correlates inversely to the length of the π-conjugated system (Table 3), with **1** having the highest solubility (>50 mg/mL). Not surprisingly, the unsubstituted fused aromatic D^1 fragments utilized for compounds **5**–**7** greatly reduce solubility. For example, the solubility of compound **6** with benzofuran units was found to be less than 10 mg/mL, whereas compound **2** with terminal hexyl bithiophene units is readily soluble up to ~35 mg/mL at room temperature. Therefore, while modifications utilizing fused planar D^1 units are effective to systematically control both the HOMO and LUMO energy levels, increasing the π-conjugated content drastically reduces solubility and, thus, may constrain the scope of conditions accessible for thin film solution deposition.

2.1. Evaluation of Different DTS (D^2) Alkyl Groups. *Synthesis.* The DTS core was modified with various solubilizing alkyl chains according to Scheme 2 to afford compounds **8** (hexyl) and **9** (dodecyl). These compounds, in conjunction with **2** (2-ethylhexyl), yield insight on the effect of the length and topology of the alkyl chains. It is worth pointing out that the length and size of the solubilizing side chains has been well established to significantly modify the properties of related -[D-A]$_n$-conjugated polymers, and thus, it is relevant to understand the degree to which these trends extend to molecular systems.[72,82–87]

2.2. Optical Characterization. Normalized absorption spectra of **2**, **8**, and **9** are shown in Figure 4a and b; see also Table 1. Compounds **2**, **8**, and **9** all exhibit λ_{max} of 625, λ_{onset} of 732 nm, and nearly identical spectral profiles in $CHCl_3$ solution. The minimal impact of alkyl chain modification in solution is expected, as each molecule contains the same chromophore unit and the conditions are sufficiently dilute to minimize multichromophore interactions. The thin film absorption spectra of **2**, **8**, and **9** display red shifts of 88, 53, and 68 nm, respectively, relative to solution spectra. Compound **2** exhibits a broader spectral width than compounds **8** and **9**. Obvious differences are observed in the spectral profiles, where **8** and **9** show better defined multiple transitions compared to **2**, which has branched side chains. This observation is in agreement with those obtained in related polymer systems, in which linear chains better interdigitate, leading to more intimate backbone contacts and enhanced electronic coupling.[72,88–90] Therefore, it is clear that the size and nature of the alkyl chains do not influence the solution absorption spectra, but bear a significant impact when the molecules are deposited as thin films. These differences likely arise from altered packing in the solid state.

2.3. Electrochemical Characterization. CV traces for compounds **2**, **8**, and **9** are shown in Figure 4c. Relevant data are provided in Table 2. No significant differences are observed in either the HOMO or LUMO energy levels. Such an observation is not surprising, since the alkyl substituents on the bridging silicon atom are removed from the main electronically delocalized framework where redox processes take place. Changes in the HOMO and LUMO levels may be observed in the solid state, where interchromophore delocalization occurs.[17] These changes are also likely to be dependent on the deposition method and the thermal history of the films.

2.4. Thermal Characterization. DSC traces for **2**, **8**, and **9** are shown in Figure 4d; see also Table 3. Melting transitions of 210, 215, and 160 °C were observed for compounds **2**, **8**, and **9**, respectively. Therefore, as the number of carbon atoms increases, lower temperatures are required to induce melting. A similar effect is observed with the crystallization temperatures: 169 °C (**2**), 185 °C (**8**), and 124 °C (**9**). This dependence of the crystallization temperature on the size of the alkyl chain is a bit surprising, especially for **2** (branched alkyl chains), in which more disorder and lower crystallization temperatures may be expected relative to **9**. Despite these uncertainties, specific information on the crystallization temperatures as a function of molecular structure is relevant for management of thin film properties via thermal annealing protocols. This represents a possible advantage over conjugated polymer counterparts, in which the amorphous nature can hide relevant features. All compounds showed good thermal stability, with 5% decomposition temperatures above 400 °C. As shown in Table 3, the solubility in $CHCl_3$ increases with the size of the alkyl chains. However, the solubilities of compounds **2** and **9** are similar, reflecting the greatly enhanced solubility imparted by the branched 2-ethylhexyl units on a per-carbon basis.[91]

3.1. Evaluation of D^2 Variations. *Synthesis.* In addition to the DTS donor core, benzodithiophene (BDT) and cyclopentadithiophene (CDT) fragments[29] were also employed as D^2. These molecules are shown as compounds **10** and **11** in Scheme 3, which also displays the general strategy for their

dx.doi.org/10.1021/ja209331y | J. Am. Chem. Soc. 2012, 134, 3766–3779

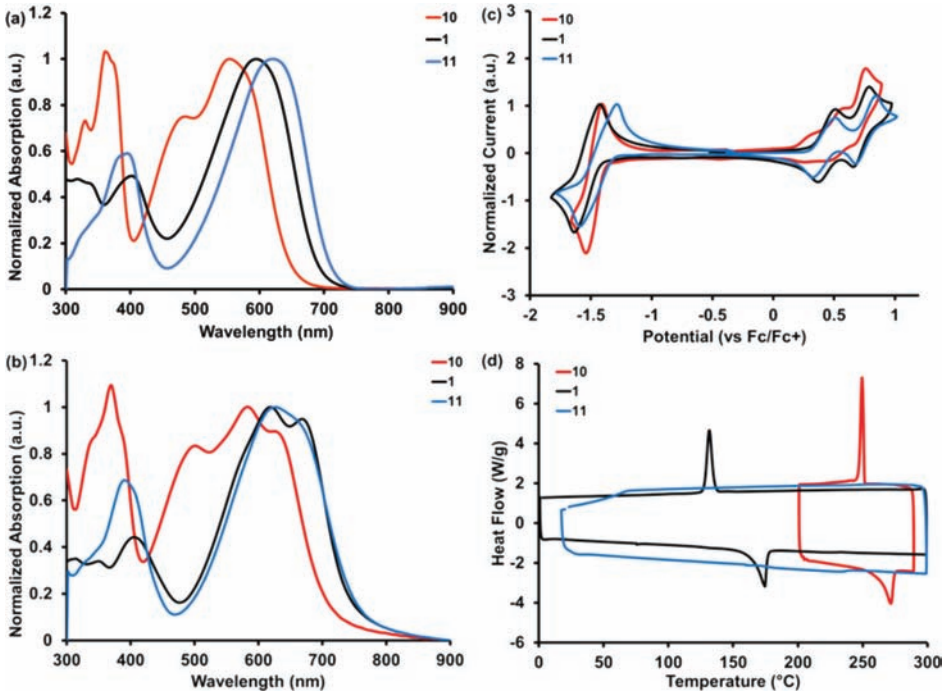

Figure 5. (a) Normalized optical absorption spectra of **1**, **10**, and **11** in (a) $CHCl_3$ solution and (b) thin films on quartz. (c) Cyclic voltammetry plots obtained in CH_2Cl_2 solution. (d) Differential scanning calorimetry plots of molecules containing varying D^2 donor cores.

synthesis. Comparison of **1**, **10**, and **11** allows one to gauge the influence of D^2 while keeping the PT-D^1 components constant. It is worth pointing out that, for polymers, the C for Si substitution can lead to significant modification of the bulk optical and electronic properties.[92−95] Such effects have yet to be investigated in molecular systems. Introducing BDT instead of DTS as a core unit, i.e. **10** vs **1**, extends the effective π-conjugation length and increases the overall molecular planarity.[96]

3.2. Optical Characterization. Solution and thin film absorption spectra of **1**, **10**, and **11** are provided in Figure 5; see also Table 1. From the solution absorbance in Figure 5a, one finds λ_{max} values of 600 nm (**1**), 555 nm (**10**), and 620 nm (**11**) and λ_{onset} values of 690 nm (**1**), 650 nm (**10**), and 715 nm (**11**). These trends are similar to those observed in analogous polymer systems.[72,93,97] In solution, the more planar and rigid structure of **10** leads to vibronic fine structure that is not observed in the profiles of **1** and **11**. Examination of solid state samples reveals λ_{onset} shifts of 70, 65, and 45 nm for **1**, **10**, and **11**, respectively, relative to solution measurements. Interestingly, **1** and **11** exhibit similar values of λ_{max} and λ_{onset} in the solid state, even though **11** exhibits a blue-shifted solution absorption. A plausible explanation for this observation may be greater molecular order in **1**, which leads to better interchromophore electronic coupling. This notion is consistent with literature findings where polymers containing Si bridged bithiophenes showed a higher degree of solid-state crystallinity compared to C bridged bithiophene.[92−94] Note also that the film absorption profile of **1** shows multiple well-defined transitions, whereas that of **11** remains broad. Solid samples of **10** also show multiple low energy transitions, not surprising given the planar structure and lack of a tetrahedral center in the internal D^2 fragment, both of which improve interchromophore interactions.

3.3. Electrochemical Characterization. CV traces of **1**, **10**, and **11** can be found in Figure 5c. Relevant data are presented in Table 2. Compounds **1** and **11** show two reversible oxidation peaks and one reversible reduction peak. However, the oxidation peak for compound **10** is only quasi-reversible. The LUMO energies were estimated at −3.47, −3.51, and −3.59 eV for **1**, **10**, and **11**, respectively. The observation that these values are similar to those of **1**−**9** further consolidates that the LUMO is largely dominated by the electronic features of the PT fragment. The HOMO energy levels were determined to be −5.20 eV (**1**), −5.23 eV (**10**), and −5.17 eV (**11**), as estimated from the onset of the first one electron oxidation peak. For **10**, several solution conditions were employed (see Supporting Information); however, the CV traces reproducibly displayed a small shoulder at lower potentials on the first oxidation peak. To the best of our knowledge, this is the first small molecule reported incorporating BDT, and at this point, it is unclear whether this feature is specific to **10** or whether this feature also exists for other BDT-containing systems. Evaluation of CV traces reported in the literature for related polymeric systems provides insufficient insight into this phenomenon, as such measurements are typically performed on thin films that yield broad and featureless oxidation waves.[96,98] From Tables 1 and 2, one sees that the electrochemical band gaps of **1**, **10**, and **11** are in agreement with the trends observed via optical absorption spectroscopy. On the basis of these electrochemical measurements, compounds **1** and **10** possess deeper HOMO energy levels and, thus, should be most likely to provide higher open circuit voltages in OPV devices when using fullerene-based acceptors.[41]

3.4. Thermal Characterization and Solubility Measurements. From the DSC traces in Figure 5d, one observes that **1** and **10** show melting transitions at 173 and 270 °C, respectively; see also Table 3. The much higher melting point of **10** may be attributed to its more planar structure, which should allow more tightly packed domains. For compound **11**, a melting transition can be observed at 110 °C during the first heating cycle (Supporting Information), but

dx.doi.org/10.1021/ja209331y | J. Am. Chem. Soc. 2012, 134, 3766−3779

Scheme 4. (a) Investigation of Regioisomers; (b) Synthetic Entry into Asymmetric Compound 13[a]

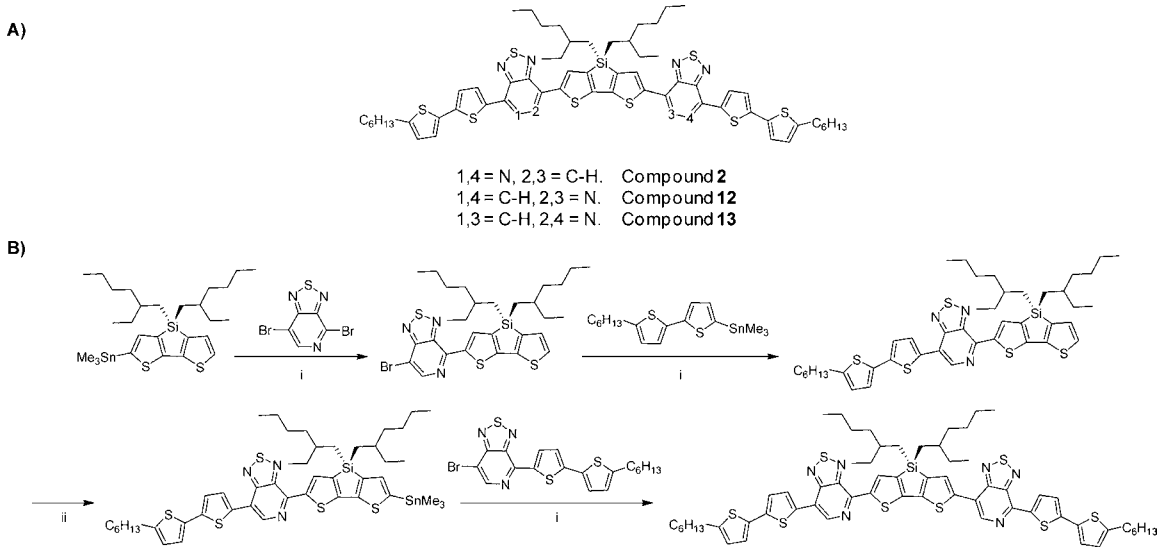

[a]Conditions: (i) Microwave reaction, 175 °C, 60 min, cat. $Pd(PPh_3)_4$, toluene. (ii) LDA, Me_3SnCl.

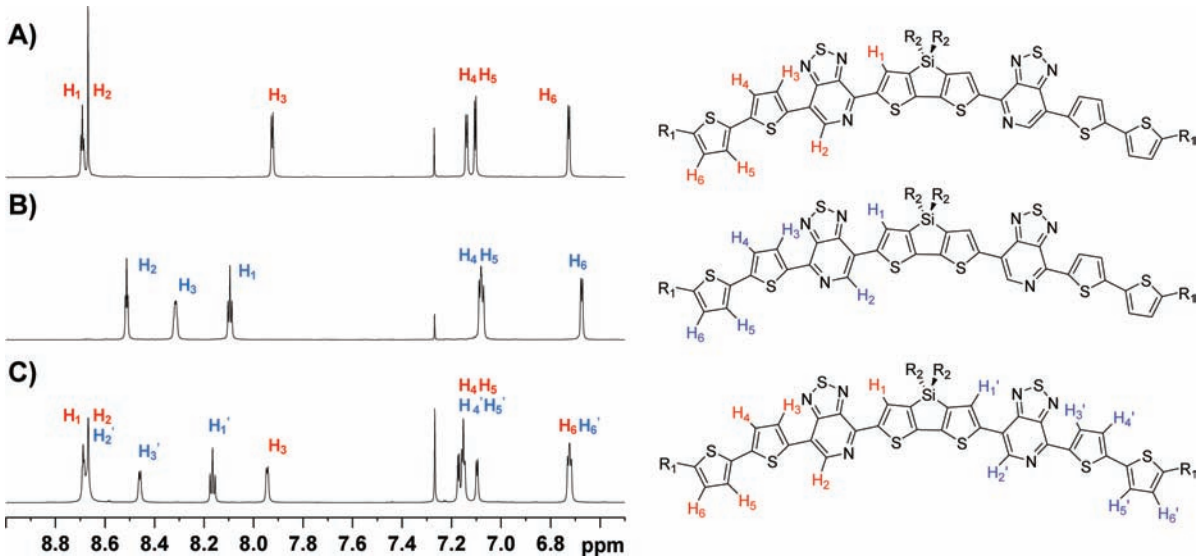

Figure 6. Aromatic region of the ^{1}H NMR spectra of (A) **12**, (B) **2**, and (C) **13**: R_1 = hexyl; R_2 = 2-ethylhexyl. Resonances at δ7.27 ppm attributed to $CHCl_3$.

upon cooling, no recrystallization was observed in subsequent heating and cooling cycles. The different behavior of **1** and **11** is especially interesting in view of their nearly identical molecular structures. At this point we do not have a complete understanding as to why such a subtle structural difference leads to such different properties, but we recognize that similar observations have been made for polymer systems, where C for Si substitution has been shown to change the thin film morphology.[72,92,94] Similar to **1**, compound **11** has good thermal stability, with 5% decomposition at 396 °C. However, compound **10** begins to decompose at a lower temperature (351 °C). Considering that all three molecules contain the same -A-D^1 segment, it is evident that the BDT core leads to instability relative to the CDT or DTS counterparts.[97] Compounds **1** and **11** are soluble above 50 mg/mL in $CHCl_3$, whereas the BDT core in compound **10** decreases the solubility to around 20 mg/mL.

4. Regiochemistry of PT in D^1-PT-D^2-PT-D^1. As a final and more subtle structural consideration, we examine how the regiochemistry of the PT unit within the overall chromophore structure impacts relevant molecular properties. Recent publications have featured compounds **2**,[66] which contains the N-atoms distal to the DTS core, and **12**,[67] which contains the N-atoms proximal to the DTS core, and under the processing conditions employed therein, **12** performed better as a donor when blended with $PC_{71}BM$ in BHJ solar cell devices. The synthesis of compound **13** was therefore designed as shown in Scheme 4. In **13** one finds one distal and one proximal N-atom, relative to DTS. A comparison of these three regioisomers was made by ^{1}H NMR spectroscopy. The aromatic regions of the ^{1}H NMR spectra of compounds **2**, **12**, and **13** are shown in Figure 6. For **12**, the pyridal N-atoms are located proximal to the central DTS unit. As a result of the electron withdrawing ability of the pyridal N-atom, both the proton resonances on the DTS (H_1) and PT (H_2) units are

dx.doi.org/10.1021/ja209331y | J. Am. Chem. Soc. 2012, 134, 3766−3779

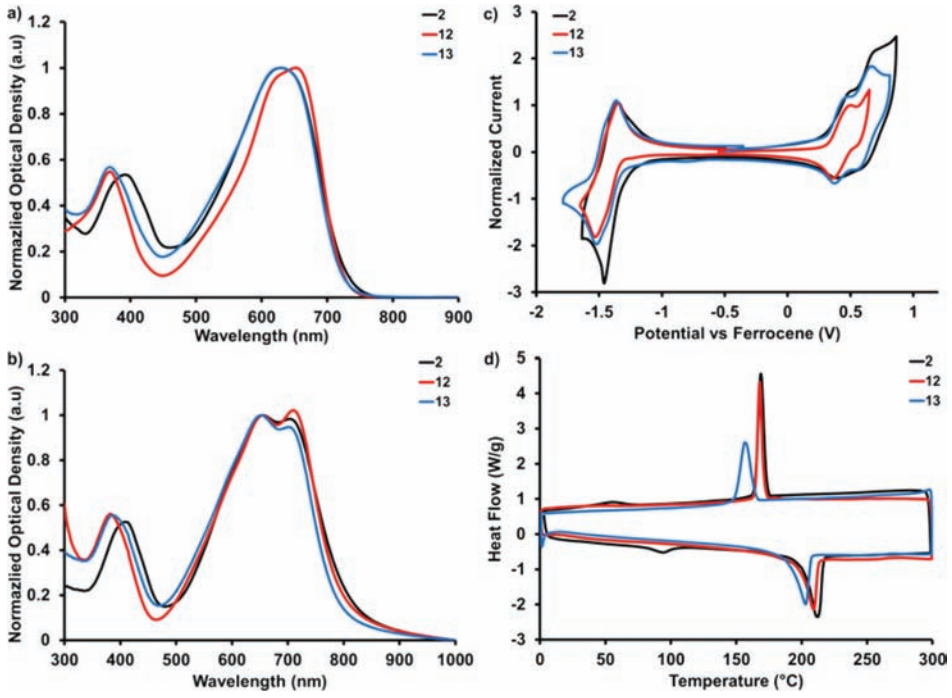

Figure 7. (a) Normalized optical absorption spectra of **2**, **12**, and **13** in (a) $CHCl_3$ solution and (b) thin films on quartz. (c) Cyclic voltammetry plots obtained in CH_2Cl_2 solution. (d) Differential scanning calorimetry of molecules with varying pyridal-N regiochemistry.

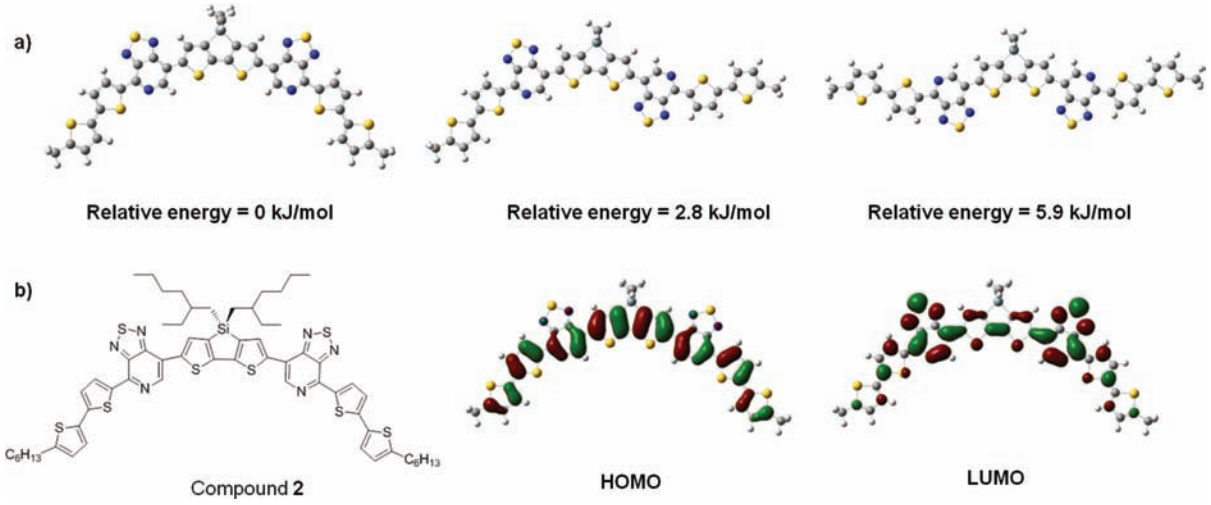

Figure 8. (a) DFT prediction of relative energies of three conformational isomers of **2**, confirming optimized geometry. (b) Representative HOMO and LUMO orbital energy diagrams of compound **2**.

shifted furthest downfield. In the case of **2**, the pyridal N-atoms are distal to the DTS unit, and as a result, the PT (H_2) proton resonances and the thiophene resonance (H_3) adjacent to the PT unit are furthest shifted downfield. The thiophene proton resonances H_4, H_5, and H_6 on the terminus of the molecule are largely unaffected by the position of the pyridal N-atom. Most importantly, the DTS proton resonances are shifted by 0.56 ppm depending on the position of the pyridal N-atom, indicating that the PT regiochemistry influences how functional groups interact with each other within the molecule. Asymmetric compound **13** exhibits at least 10 distinct proton resonances, compared to 6 aromatic resonances for the symmetric **2** and **12**, and is virtually a combination of the spectra of **2** and **12**.

In the solution absorption spectrum (Figure 7a), the λ_{max} of **12** is slightly red-shifted relative to **2** or **13**, potentially due to a planarization of the core induced by N---S interactions between PT and DTS.[66,99,100] This is further corroborated by the enhanced low energy peak in the thin film spectra (Figure 7b). All three compounds exhibit similar oxidation and reduction potentials in solution (Figure 7c, Table 2). Finally, **13** exhibits slightly lower melting and crystallization temperatures. The fact that **2** and **12** exhibit similar optical, electrochemical, and thermal properties, yet have been reported to give different performance in BHJ solar cells (PCE = 3.2%[66] and 6.7%,[67] respectively) highlights the limitations of molecular design and the importance of processing conditions and overall device configuration and fabrication in realizing the full potential of a given material. It is likely that under appropriate conditions

dx.doi.org/10.1021/ja209331y | J. Am. Chem. Soc. 2012, 134, 3766–3779

compounds **2**, **12**, and **13** would perform similarly in optoelectronic devices.

5. Theoretical Examination and Summary of Structural Trends. Density functional theory (DFT) calculations using the hybrid B3LYP exchange-correlation functional and the split-valence 6-31G(d,p) basis set were used to investigate the conformational and electronic properties of compounds **1**−**13**. DFT calculations are useful for predicting optimized structures, confirming molecular geometry, verifying complete delocalization across the conjugated backbones, and predicting electronic energy levels.[101] Initial calculations were performed using **2** with various PT acceptor orientations in order to determine the lowest energy conformation (Figure 8a). Three orientations were analyzed: both acceptor PT units with the pyridal N-atom *trans* to the Si-atom (left), PT units in opposite orientations (middle), and PT units with the pyridal N-atom *cis* to the Si-atom (right). Consistent with the graphical depiction of **2** in Figure 1 and Scheme 2, the lowest energy conformational isomer is nearly coplanar and adopts a bent, "banana" type structure.[102,103] All the calculations of **1**−**13** were carried out by relying on such a bent conformation. As a representative example, the optimized structures and HOMO and LUMO orbital diagrams for **2** are shown in Figure 8. One observes full delocalization of HOMO and LUMO across the molecular backbone. Please refer to the Supporting Information for similar results for all the other compounds. A side-by-side comparison of experimental and theoretical HOMO and LUMO energy values is presented in the Supporting Information; a summary is provided in Table 2. From these results it is evident that for this class of compounds DFT calculations at the current level of theory can provide only general trends and fail to predict the effect of more subtle structural modifications. DFT calculations nonetheless successfully confirmed the molecular geometry and indicate extended delocalization of the frontier molecular orbital levels. The database of experimentally determined properties reported herein thus provides a useful benchmark to gauge the precision of different computational approaches.

■ CONCLUSION

Thirteen different D^1-A-D^2-A-D^1 chromophores based on the PT heterocycle as the acceptor "A" unit were synthesized and characterized by using a variety of techniques to obtain a comprehensive experimental framework from which to derive structure−property relationships, at least at the molecular and single component level. The modular nature of the molecular architecture allows straightforward access to a range of derivatives that allow one to isolate the influence of each building block on molecular properties. It is worth highlighting that similar insight with related conjugated polymers is less precise on account of variations in molecular weight, differences in polydispersities, and the fact that a wider range of local environments can be found. A summary of relevant findings follows.

From electrochemical measurements and DFT calculations one finds that in all thirteen D^1-PT-D^2-PT-D^1 molecules, the energy levels and the spatial distribution of the LUMOs are dominated by the PT fragment. Variations of the end-cap D^1 units and the central D^2 aromatic core can be used to modify optical absorption, to optimize harvesting of the solar spectrum and HOMO energy levels, and ultimately to improve the open circuit voltages of the solar cells. Comparison of compounds **1**, **2**, and **3** shows that the influence of the number of thiophene repeat units on the optical absorption saturates with two thiophene moieties. It is also worth noting that, on the basis of the sharpness of the features in the solid state absorption spectra, one finds that compound **2** produced more ordered as cast films compared to **1** and **3**.

Compounds **4**, **5**, **6**, and **7** with unsubstituted thiophene, benzothiophene, benzofuran, and benzothiazole D^1 end groups, respectively, exhibit favorable optical properties suitable for harvesting sunlight, but they are likely to be more difficult to process given their lower solubilities, relative to derivatives bearing terminal hexyl groups, i.e. **1**, **2**, and **3**. Modifications of the D^1 units in **5**, **6**, and **7** with additional solubilizing groups will be required to circumvent this problem and possibly include these molecular frameworks into useful devices. It was unexpected to find that compound **7** exhibits difficulty in crystallizing, as determined by DSC. The presence of a broad thin film absorption spectrum of **7** is consistent with this observation. These observations show the limitations of molecular-level engineering for fully predicting solid state behavior and, particularly, interchromophore organization. It is reasonable to anticipate that using solvents that evaporate more slowly, high boiling additives, or thermal annealing could be ways to introduce more order.

From examination of compounds **2** (2-ethylexyl), **8** (hexyl), and **9** (dodecyl), one can confirm that the nature of the alkyl groups on the dithieno(3,2-*b*;2′,3′-*d*)silole (DTS) internal core does not influence the optical and electrochemical properties in solution. We recognize that this is not a surprising observation given that these substituents are not an integral component of the π-delocalized framework. The solid state absorption, however, shows a broader band for **2**, relative to **8** and **9**, indicating a greater diversity of environments in the thin film. From a practical perspective, the larger dodecyl and 2-ethylexyl groups make the molecules more soluble than the hexyl counterpart and are, therefore, more likely to be processed into continuous thin films, at least by spin coating techniques. However, that the 2-ethylexyl substituent imparts a 50 °C increase in the melting temperature, relative to dodecyl, is unexpected and highlights that this solubilizing group may ultimately lead to more thermally stable materials. The 2-ethylexyl group appears to be therefore a more desirable initial choice when considering future elaboration of new small molecules with optical and electronic features fine-tuned by the π-conjugated framework.

Differences in the nature of the D^2 core reveal some relevant features. The simple isoelectronic Si (DTS) for C (CDT) substitution in compounds **1** and **11**, respectively, yields a red shift in absorption for the C-based system, but only in solution. The wavelength ranges covered by absorption in the solid state are similar to each other. For reasons that remain poorly understood, the thermal behaviors of **1** and **11** are quite different, as shown by DSC. Such different properties are not possible to predict *a priori*, again pointing out important deficiencies in understanding how weak forces come together to determine the solid state morphology. Moreover, it was found that the benzodithiophene (BDT) for D^2 in **10** leads to a significant blue shift in absorption, relative to **1**, which is consistent with less pronounced charge transfer characteristics and, therefore, a weaker donor core. By looking at the thermal properties of **10**, one finds that the more planar BDT framework leads to the highest melting temperature, compared to DTS or CDT. This stability is brought at the expense of lower thermal decomposition temperatures, although it is not

clear at this stage if this instability is an intrinsic feature of BDT. It will be of interest to see if replacement of the alkoxy groups for alkyl counterparts can be used for increasing the decomposition temperature.

Compounds **2**, **12**, and **13** provide all the possible regiochemical isomers with respect to the orientation of the PT heterocycle relative to the internal DTS donor core. The pyridal N can be proximal, i.e. pointing toward DTS, or distal, i.e. pointing away from DTS. Thus, **2** corresponds to the distal, distal species, while **12** and **13** are the proximal, proximal and distal, proximal regioisomers, respectively. The sequence in Scheme 4 for the preparation of **13** is worth noting, in that the number of chemical steps and purification procedures is considerably increased when asymmetric species are desired; this complexity must be compensated by desirable physical properties in order to warrant the upfront synthetic effort. We find that the absorption features and electrochemical properties of **2**, **12**, and **13** are indistinguishable within experimental error. Compound **13**, however, melts at a slightly lower temperature, 202 °C, relative to **2** (210 °C) and **12** (207 °C). Given the above characteristics of **2**, **12**, and **13**, there is little evidence at this point that either of these molecules would be a more preferred candidate for incorporation into functioning devices.

As a final note, we point out that the majority of BHJ solar cells in the literature, including some of the highest performing conjugated polymers, have been fabricated via spin coating techniques. Such a method is not as amenable for high throughput production as other techniques, for example roll-to-roll processing and/or printing. This perspective suggests that perhaps less soluble D^1-A-D^2-A-D^1 chromophores with planar heterocyclic aromatic end groups, i.e. **5**, **6**, and **7**, may increase in practical relevance if the fabrication methods can tolerate higher temperatures or more dilute conditions. The work presented in this contribution provides guidelines for tailoring molecular materials that may be suitable once the more preferred device fabrication method has been determined.

■ ASSOCIATED CONTENT

Supporting Information

Methods and materials, synthesis and spectroscopic characterization of all compounds, solution ^{1}H NMR spectra, absorption spectra of thermally annealed films, TGA plots, CV plots for compound **10** in different solvents, DFT optimized structures, and HOMO/LUMO representations. This material is available free of charge via the Internet at http://pubs.acs.org.

■ AUTHOR INFORMATION

Corresponding Author

bazan@chem.ucsb.edu

Author Contributions

[#]Authors contributed equally.

Notes

The authors declare no competing financial interest.

■ ACKNOWLEDGMENTS

We thank the Office of Naval Research (N-00014-04-0411 for materials synthesis) and the Center for Energy Efficient Materials, an Energy Frontier Research Center funded by the Office of Basic Energy Sciences of the U.S. Department of Energy (DE-DC0001009 for support of G.C.W. and T.v.d.P.) for supporting this work.

■ REFERENCES

(1) Kippelen, B.; Bredas, J. L. *Energy Environ. Sci.* **2009**, *2*, 251.
(2) Veinot, J. G. C.; Marks, T. J. *Acc. Chem. Res.* **2005**, *38*, 632.
(3) Chen, C.-T. *Chem. Mater.* **2004**, *16*, 4389.
(4) Haldi, A.; Kimyonok, A.; Domercq, B.; Hayden, L. E.; Jones, S. C.; Marder, S. R.; Weck, M.; Kippelen, B. *Adv. Funct. Mater.* **2008**, *18*, 3056.
(5) Murphy, A. R.; Fréchet, J. M. J. *Chem. Rev.* **2007**, *107*, 1066.
(6) Usta, H.; Facchetti, A.; Marks, T. J. *Acc. Chem. Res.* **2011**, *44*, 501.
(7) Dong, H.; Wang, C.; Hu, W. *Chem. Commun.* **2010**, *46*, 5211.
(8) Dennler, G.; Scharber, M. C.; Brabec, C. J. *Adv. Mater.* **2009**, *21*, 1323.
(9) Cheng, Y. J.; Yang, S. H.; Hsu, C. S. *Chem. Rev.* **2009**, *109*, 5868.
(10) Zeng, W.; Cao, Y.; Bai, Y.; Wang, Y.; Shi, Y.; Zhang, M.; Wang, F.; Pan, C.; Wang, P. *Chem. Mater.* **2010**, *22*, 1915.
(11) Thomas, S. W.; Joly, G. D.; Swager, T. M. *Chem. Rev.* **2007**, *107*, 1339.
(12) Argun, A. A.; Cirpan, A.; Reynolds, J. R. *Adv. Mater.* **2003**, *15*, 1338.
(13) Beaujuge, P. M.; Ellinger, S.; Reynolds, J. R. *Nat. Mater.* **2008**, *7*, 795.
(14) Beaujuge, P. M.; Reynolds, J. R. *Chem. Rev.* **2010**, *110*, 268.
(15) Gong, X.; Tong, M.; Xia, Y.; Cai, W.; Moon, J. S.; Cao, Y.; Yu, G.; Shieh, C.-L.; Nilsson, B.; Heeger, A. J. *Science* **2009**, *325*, 1665.
(16) Peumans, P.; Yakimov, A.; Forrest, S. R. *J. Appl. Phys.* **2003**, *93*, 3693.
(17) Lin, L.-Y.; Chen, Y.-H.; Huang, Z.-Y.; Lin, H.-W.; Chou, S.-H.; Lin, F.; Chen, C.-W.; Liu, Y.-H.; Wong, K.-T. *J. Am. Chem. Soc.* **2011**, *133*, 15822.
(18) Wei, G.; Wang, S.; Sun, K.; Thompson, M. E.; Forrest, S. R. *Advanced Energy Materials* **2011**, *1*, 184.
(19) Steinmann, V.; Kronenberg, N. M.; Lenze, M. R.; Graf, S. M.; Hertel, D.; Meerholz, K.; Bürckstümmer, H.; Tulyakova, E. V.; Würthner, F. *Advanced Energy Materials* **2011**, *1*, 888.
(20) Zhong, C.; Duan, C.; Huang, F.; Wu, H.; Cao, Y. *Chem. Mater.* **2010**, *23*, 326.
(21) Brabec, C. J.; Gowrisanker, S.; Halls, J. J. M.; Laird, D.; Jia, S.; Williams, S. P. *Adv. Mater.* **2010**, *22*, 3839.
(22) Sekitani, T.; Someya, T. *Adv. Mater.* **2010**, *22*, 2228.
(23) Forrest, S. R. *Nature* **2004**, *428*, 911.
(24) Hübler, A.; Trnovec, B.; Zillger, T.; Ali, M.; Wetzold, N.; Mingebach, M.; Wagenpfahl, A.; Deibel, C.; Dyakonov, V. *Adv. Energy Mater.* **2011**, *1*, 1018.
(25) Beaujuge, P. M.; Amb, C. M.; Reynolds, J. R. *Acc. Chem. Res.* **2010**, *43*, 1396.
(26) Wang, S.; Oldham, W. J.; Hudack, R. A.; Bazan, G. C. *J. Am. Chem. Soc.* **2000**, *122*, 5695.
(27) Holcombe, T. W.; Norton, J. E.; Rivnay, J.; Woo, C. H.; Goris, L.; Piliego, C.; Griffini, G.; Sellinger, A.; Brédas, J.-L.; Salleo, A.; Fréchet, J. M. J. *J. Am. Chem. Soc.* **2011**, *133*, 12106.
(28) Roncali, J. *Macromol. Rapid Commun.* **2007**, *28*, 1761.
(29) Gendron, D.; Leclerc, M. *Energy Environ. Sci.* **2011**, *4*, 1225.
(30) Amb, C. M.; Chen, S.; Graham, K. R.; Subbiah, J.; Small, C. E.; So, F.; Reynolds, J. R. *J. Am. Chem. Soc.* **2011**, *133*, 10062.
(31) Zhou, H.; Yang, L.; Stuart, A. C.; Price, S. C.; Liu, S.; You, W. *Angew. Chem., Int. Ed.* **2011**, *50*, 2995.
(32) Price, S. C.; Stuart, A. C.; Yang, L.; Zhou, H.; You, W. *J. Am. Chem. Soc.* **2011**, *133*, 4625.
(33) He, Z.; Zhong, C.; Huang, X.; Wong, W.-Y.; Wu, H.; Chen, L.; Su, S.; Cao, Y. *Adv. Mater.* **2011**, *23*, 4636.
(34) Chu, T.-Y.; Lu, J.; Beaupré, S.; Zhang, Y.; Pouliot, J.-R. m.; Wakim, S.; Zhou, J.; Leclerc, M.; Li, Z.; Ding, J.; Tao, Y. *J. Am. Chem. Soc.* **2011**, *133*, 4250.
(35) Zhang, W.; Smith, J.; Watkins, S. E.; Gysel, R.; McGehee, M.; Salleo, A.; Kirkpatrick, J.; Ashraf, S.; Anthopoulos, T.; Heeney, M.; McCulloch, I. *J. Am. Chem. Soc.* **2010**, *132*, 11437.
(36) Zhang, M.; Tsao, H. N.; Pisula, W.; Yang, C.; Mishra, A. K.; Müllen, K. *J. Am. Chem. Soc.* **2007**, *129*, 3472.

(37) Tsao, H. N.; Cho, D. M.; Park, I.; Hansen, M. R.; Mavrinskiy, A.; Yoon, D. Y.; Graf, R.; Pisula, W.; Spiess, H. W.; Müllen, K. *J. Am. Chem. Soc.* **2011**, *133*, 2605.
(38) Bijleveld, J. C.; Shahid, M.; Gilot, J.; Wienk, M. M.; Janssen, R. A. J. *Adv. Funct. Mater.* **2009**, *19*, 3262.
(39) Bijleveld, J. C.; Zoombelt, A. P.; Mathijssen, S. G. J.; Wienk, M. M.; Turbiez, M.; de Leeuw, D. M.; Janssen, R. A. J. *J. Am. Chem. Soc.* **2009**, *131*, 16616.
(40) Bijleveld, J. C.; Gevaerts, V. S.; Di Nuzzo, D.; Turbiez, M.; Mathijssen, S. G. J.; de Leeuw, D. M.; Wienk, M. M.; Janssen, R. A. J. *Adv. Mater.* **2010**, *22*, E242.
(41) Walker, B.; Kim, C.; Nguyen, T.-Q. *Chem. Mater.* **2010**, *23*, 470.
(42) Roncali, J. *Acc. Chem. Res.* **2009**, *42*, 1719.
(43) Li, Y.; Guo, Q.; Li, Z.; Pei, J.; Tian, W. *Energy Environ. Sci.* **2010**, *3*, 1427.
(44) Riede, M.; Mueller, T.; Tress, W.; Schueppel, R.; Leo, K. *Nanotechnology* **2008**, *19*, 424001.
(45) Tamayo, A. B.; Tantiwiwat, M.; Walker, B.; Nguyen, T.-Q. *J. Phys. Chem. C* **2008**, *112*, 15543.
(46) Fitzner, R.; Reinold, E.; Mishra, A.; Mena-Osteritz, E.; Ziehlke, H.; Körner, C.; Leo, K.; Riede, M.; Weil, M.; Tsaryova, O.; Weiß, A.; Uhrich, C.; Pfeiffer, M.; Bäuerle, P. *Adv. Funct. Mater.* **2011**, *21*, 897.
(47) Burckstummer, H.; Kronenberg, N. M.; Meerholz, K.; Wurthner, F. *Org. Lett.* **2010**, *12*, 3666.
(48) Burckstummer, H.; Kronenberg, N. M.; Gsanger, M.; Stolte, M.; Meerholz, K.; Wurthner, F. *J. Mater. Chem.* **2010**, *20*, 240.
(49) Bagnis, D.; Beverine, L.; Huang, H.; Silvestri, F.; Yao, Y.; Yan, H.; Pagani, G. A.; Marks, T. J.; Facchetti, A. *J. Am. Chem. Soc.* **2010**, *132*, 4074.
(50) Mayerhoffer, U.; Deing, K.; Gruss, K.; Braunschweig, H.; Meerholz, K.; Wurthner, F. *Angew. Chem., Int. Ed.* **2009**, *48*, 8776.
(51) Wei, G. D.; Wang, S. Y.; Renshaw, K.; Thompson, M. E.; Forrest, S. R. *ACS Nano* **2010**, *4*, 1927.
(52) Wei, G. D.; Lunt, R. R.; Sun, K.; Wang, S. Y.; Thompson, M. E.; Forrest, S. R. *Nano Lett.* **2010**, *10*, 3555.
(53) Rousseau, T.; Cravino, A.; Bura, T.; Ulrich, G.; Ziessel, R.; Roncali, J. *Chem. Commun.* **2009**, 1673.
(54) Rousseau, T.; Cravino, A.; Bura, T.; Ulrich, G.; Ziessel, R.; Roncali, J. *J. Mater. Chem.* **2009**, *19*, 2298.
(55) Rousseau, T.; Cravino, A.; Ripaud, E.; Leriche, P.; Rihn, S.; De Nicola, A.; Ziessel, R.; Roncali, J. *Chem. Commun.* **2010**, *46*, 5082.
(56) Mei, J. G.; Graham, K. R.; Stalder, R.; Reynolds, J. R. *Org. Lett.* **2010**, *12*, 660.
(57) Loser, S.; Bruns, C. J.; Miyauchi, H.; Ortiz, R. o. P.; Facchetti, A.; Stupp, S. I.; Marks, T. J. *J. Am. Chem. Soc.* **2011**, *133*, 8142.
(58) Walker, B.; Tomayo, A. B.; Dang, X. D.; Zalar, P.; Seo, J. H.; Garcia, A.; Tantiwiwat, M.; Nguyen, T. Q. *Adv. Funct. Mater.* **2009**, *19*, 3063.
(59) Yin, B.; Yang, L. Y.; Liu, Y. S.; Chen, Y. S.; Qi, Q. J.; Zhang, F. L.; Yin, S. G. *Appl. Phys. Lett.* **2010**, *97*, 3.
(60) Liu, Y. S.; Wan, X. J.; Yin, B.; Zhou, J. Y.; Long, G. K.; Yin, S. G.; Chen, Y. S. *J. Mater. Chem.* **2010**, *20*, 2464.
(61) Liu, Y.; Wan, X.; Wang, F.; Zhou, J.; Long, G.; Tian, J.; You, J.; Yang, Y.; Chen, Y. *Adv. Energy Mater.* **2011**, *1*, 771.
(62) Zhang, F.; Wu, D.; Xu, Y.; Feng, X. *J. Mater. Chem.* **2011**, *21*, 17590.
(63) Shang, H.; Fan, H.; Liu, Y.; Hu, W.; Li, Y.; Zhan, X. *Adv. Mater.* **2011**, *23*, 1554.
(64) Zhang, J.; Deng, D.; He, C.; He, Y.; Zhang, M.; Zhang, Z.-G.; Zhang, Z.; Li, Y. *Chem. Mater.* **2010**, *23*, 817.
(65) Ko, H. M.; Choi, H.; Paek, S.; Kim, K.; Song, K.; Lee, J. K.; Ko, J. *J. Mater. Chem.* **2011**, *21*, 7248.
(66) Welch, G. C.; Perez, L. A.; Hoven, C. V.; Zhang, Y.; Dang, X.-D.; Sharenko, A.; Toney, M. F.; Kramer, E. J.; Nguyen, T.-Q.; Bazan, G. C. *J. Mater. Chem.* **2011**, *21*, 12700.
(67) Sun, Y.; Welch, G. C.; Leong, W. L.; Takacs, C. J.; Bazan, G. C.; Heeger, A. J. *Nat. Mater.* **2011**, *11*, 44.
(68) Peet, J.; Heeger, A. J.; Bazan, G. C. *Acc. Chem. Res.* **2009**, *42*, 1700.
(69) Peet, J.; Senatore, M. L.; Heeger, A. J.; Bazan, G. C. *Adv. Mater.* **2009**, *21*, 1521.
(70) Wienk, M. M.; Turbiez, M.; Gilot, J.; Janssen, R. A. J. *Adv. Mater.* **2008**, *20*, 2556.
(71) Ying, L.; Hsu, B.; Zhan, H.; Welch, G.; Zalar, P.; Perez, L.; Kramer, E.; Nguyen, T.-Q.; Heeger, A.; Wong, W.-Y.; Bazan, G. *J. Am. Chem. Soc.* **2011**, *133*, 18538.
(72) Coffin, R. C.; Peet, J.; Rogers, J.; Bazan, G. C. *Nature Chem.* **2009**, *1*, 657.
(73) Blouin, N.; Michaud, A.; Gendron, D.; Wakim, S.; Blair, E.; Neagu-Plesu, R.; Belletete, M.; Durocher, G.; Tao, Y.; Leclerc, M. *J. Am. Chem. Soc.* **2008**, *130*, 732.
(74) Zhang, R.; Li, B.; Iovu, M. C.; Jeffries-El, M.; Sauvé, G.; Cooper, J.; Jia, S.; Tristram-Nagle, S.; Smilgies, D. M.; Lambeth, D. N.; McCullough, R. D.; Kowalewski, T. *J. Am. Chem. Soc.* **2006**, *128*, 3480.
(75) Handy, S. T.; Wilson, T.; Muth, A. *J. Org. Chem.* **2007**, *72*, 8496.
(76) Schwab, P. F. H.; Fleischer, F.; Michl, J. *J. Org. Chem.* **2002**, *67*, 443.
(77) Meier, H. *Angew. Chem., Int. Ed.* **2005**, *44*, 2482.
(78) Würthner, F.; Kaiser, T. E.; Saha-Möller, C. R. *Angew. Chem., Int. Ed.* **2011**, *50*, 3376.
(79) Kim, J. *Pure Appl. Chem.* **2002**, *74*, 2031.
(80) Steinberger, S.; Mishra, A.; Reinold, E.; Levichkov, J.; Uhrich, C.; Pfeiffer, M.; Bauerle, P. *Chem. Commun.* **2011**, *47*, 1982.
(81) Cardona, C. M.; Li, W.; Kaifer, A. E.; Stockdale, D.; Bazan, G. C. *Adv. Mater.* **2011**, *23*, 2367.
(82) Yue, W.; Zhao, Y.; Shao, S.; Tian, H.; Xie, Z.; Geng, Y.; Wang, F. *J. Mater. Chem.* **2009**, *19*, 2199.
(83) Biniek, L.; Fall, S.; Chochos, C. L.; Anokhin, D. V.; Ivanov, D. A.; Leclerc, N.; Lévêque, P.; Heiser, T. *Macromolecules* **2010**, *43*, 9779.
(84) Szarko, J. M.; Guo, J.; Liang, Y.; Lee, B.; Rolczynski, B. S.; Strzalka, J.; Xu, T.; Loser, S.; Marks, T. J.; Yu, L.; Chen, L. X. *Adv. Mater.* **2010**, *22*, 5468.
(85) Yang, L.; Zhou, H.; You, W. *J. Phys. Chem. C* **2010**, *114*, 16793.
(86) Szarko, J. M.; Guo, J.; Rolczynski, B. S.; Chen, L. X. *J. Mater. Chem.* **2011**, *21*, 7849.
(87) Subramaniyan, S.; Xin, H.; Kim, F. S.; Shoaee, S.; Durrant, J. R.; Jenekhe, S. A. *Adv. Energy Mater.* **2011**, *1*, 854.
(88) Piliego, C.; Holcombe, T. W.; Douglas, J. D.; Woo, C. H.; Beaujuge, P. M.; Frechet, J. M. J. *J. Am. Chem. Soc.* **2010**, *132*, 7595.
(89) Chabinyc, M. L.; Toney, M. F.; Kline, R. J.; McCulloch, I.; Heeney, M. *J. Am. Chem. Soc.* **2007**, *129*, 3226.
(90) Cates, N. C.; Gysel, R.; Beiley, Z.; Miller, C. E.; Toney, M. F.; Heeney, M.; McCulloch, I.; McGehee, M. D. *Nano Lett.* **2009**, *9*, 4153.
(91) Zhu, Z.; Waller, D.; Gaudiana, R.; Morana, M.; Mühlbacher, D.; Scharber, M.; Brabec, C. *Macromolecules* **2007**, *40*, 1981.
(92) Chen, H. Y.; Hou, J. H.; Hayden, A. E.; Yang, H.; Houk, K. N.; Yang, Y. *Adv. Mater.* **2010**, *22*, 371.
(93) Morana, M.; Azimi, H.; Dennler, G.; Egelhaaf, H.-J.; Scharber, M.; Forberich, K.; Hauch, J.; Gaudiana, R.; Waller, D.; Zhu, Z.; Hingerl, K.; van Bavel, S. S.; Loos, J.; Brabec, C. J. *Adv. Funct. Mater.* **2010**, *20*, 1180.
(94) Scharber, M. C.; Koppe, M.; Gao, J.; Cordella, F.; Loi, M. A.; Denk, P.; Morana, M.; Egelhaaf, H. J.; Forberich, K.; Dennler, G.; Gaudiana, R.; Waller, D.; Zhu, Z. G.; Shi, X. B.; Brabec, C. J. *Adv. Mater.* **2010**, *22*, 367.
(95) Zhang, Y.; Zou, J.; Yip, H.-L.; Sun, Y.; Davies, J. A.; Chen, K.-S.; Acton, O.; Jen, A. K. Y. *J. Mater. Chem.* **2011**, *21*, 3895.
(96) Hou, J.; Park, M.-H.; Zhang, S.; Yao, Y.; Chen, L.-M.; Li, J.-H.; Yang, Y. *Macromolecules* **2008**, *41*, 6012.
(97) Huo, L.; Hou, J.; Chen, H.-Y.; Zhang, S.; Jiang, Y.; Chen, T. L.; Yang, Y. *Macromolecules* **2009**, *42*, 6564.
(98) Liang, Y.; Xu, Z.; Xia, J.; Tsai, S.-T.; Wu, Y.; Li, G.; Ray, C.; Yu, L. *Adv. Mater.* **2010**, *22*, E135.
(99) Yasuda, T.; Sakai, Y.; Aramaki, S.; Yamamoto, T. *Chem. Mater.* **2005**, *17*, 6060.
(100) Karikomi, M.; Kitamura, C.; Tanaka, S.; Yamashita, Y. *J. Am. Chem. Soc.* **1995**, *117*, 6791.

(101) Risko, C.; McGehee, M. D.; Bredas, J.-L. *Chem. Sci.* **2011**, *2*, 1200.
(102) Pelzl, G.; Diele, S.; Weissflog, W. *Adv. Mater.* **1999**, *11*, 707.
(103) Ros, M. B.; Serrano, J. L.; de la Fuente, M. R.; Folcia, C. L. *J. Mater. Chem.* **2005**, *15*, 5093.